Hindawi
Advances in Polymer Technology
Volume 2022, Article ID 1178039, 9 pages
https://doi.org/10.1155/2022/1178039

Research Article

Mitochondria-Targeting and ROS-Responsive Nanocarriers via Amphiphilic *TPP-PEG-TK-Ce6* for Nanoenabled Photodynamic Therapy

Yangjian Wang,[1] Junshui Zheng,[2] Jian Lin,[2] Kai Ye,[2] and Peng Wei[1]

[1]*Reparative and Reconstructive Surgery, First Hospital of Ningbo, Ningbo 315000, China*
[2]*School of Medicine, Ningbo University, Ningbo, Zhejiang, 315211, China*

Correspondence should be addressed to Peng Wei; weipeng@nbu.edu.cn

Received 7 December 2021; Revised 19 March 2022; Accepted 26 March 2022; Published 13 April 2022

Academic Editor: Li Zibiao

Designing targeted-delivering and stimuli-responsive nanocarriers for photodynamic therapy (PDT) is an appealing method, especially, targeting delivery of photosensitizers to mitochondria as the most sensitive cellular organelles to reactive oxygen species (ROS) could significantly enhance the therapeutic efficacy of PDT. In this study, we synthesized triphenylphosphonium bonded PEG-NH_2 (TPP-PEG-NH_2) and bridged to chlorin e6 (Ce6) via thioketal (TK) linkage to obtain red light-triggered, amphiphilic copolymer (TPP-PEG-TK-Ce6), which could self-assemble into micelles with an average size of 160 nm and zeta potential of +20.1 mV. The *in vitro* release behavior of TPP-PEG-TK-Ce6 nanocarriers showed a light-activated way and was dependent on the H_2O_2 concentration. TPP-PEG-TK-Ce6 nanocarriers exhibited high cytotoxicity against C6 cells with illumination. Confocal laser scanning microscopy observation indicated that TPP-PEG-TK-Ce6 nanocarriers were efficiently internalized into the mitochondrion of C6 cells, released Ce6 via light activated. By contrast, in the case of TPP-PEG-NH_2 directly bonded Ce6 (TPP-PEG-Ce6) nanocarriers, little Ce6 was found in the mitochondrion. The stronger fluorescence in the mitochondrion of TPP-PEG-TK-Ce6 nanocarriers originated from the mitochondrial-targeting capability of TPP and the cleavage of TK linkages activated by light irradiation, which greatly improved the cellular uptake of TPP-PEG-TK-Ce6 nanocarriers and released more Ce6 in the mitochondrion. This work provided a facile strategy to improve PDT efficacy.

1. Introduction

Photodynamic therapy (PDT) is a photochemistry-involved treatment process that exploiting of photosensitizers (PSs), which could be light-activated by irradiation of a specific wavelength of light, to generate cytotoxic reactive oxygen species (ROS), thus causing cell apoptosis and tissue destruction [1–5]. The application of PDT is limited by short life time, tumor nonspecificity, rapid cellular elimination, and low diffusion radius of singlet oxygen (SO) [6–9]. Especially, SO that caused the death of tumor cells has a short half-life of <40 ns and could only be effective within a limited distance of <20 nm after generation [10], therefore, it is superior to deliver PSs to critical subcellular organelles with higher susceptibility to ROS not just into tumor cells [11, 12]. Mitochondria acted as the power house of cells to regulate the actions of ATP production, ROS generation, and programmed cell death (apoptosis) [13, 14]. Moreover, mitochondria dysfunction could result in a series of diseases such as Alzheimer's disease, diabetes, and cancer [15–17]. Mitochondria play a vital role in the death of cancerous cells, so directly delivering PSs into mitochondria is emerging as a preferential strategy to improve the PDT efficacy [18–20]. Many drug delivery nanocarriers that chemically modified with mitochondrial-targeting groups such as lipophilic ligand triphenylphosphonium (TPP) and zwitterionic oligopeptides [21–23] have been demonstrated to successfully deliver PSs into mitochondria of cancerous cells.

In addition, another pivotal parameter to elevate PDT efficacy is the controlled release capability of PSs of the

nanocarriers in tumor microenvironment via light activation [24]. In contrast to traditional pH, redox, enzyme, and temperature-responsive nanocarriers, ROS-responsive nanocarriers for PDT have attracted more attention as self-triggered delivery systems owing to PSs generated much ROS on light irradiation which could result in cleavage and degradation of the ROS-responsive nanocarriers. For example, thioketal (TK) linkages are readily cleaved in ROS-enriched tumor microenvironments [25–28]. The released PSs from ROS-responsive nanocarriers could further accelerate the susceptibility of exposed PSs to light for generating much more SO to kill tumor cells. Wang et al. have utilized ROS-activable thioketal (TK) bond as a linkage between doxorubicin (DOX) and polyphosphoester (PPE-TK-DOX) and constructed Ce6@PPE-TK-DOX NPs via coself-assembly, which were stable in physiological conditions and could induce localized ROS generation resulting in rapid cleavage of the TK bond via illumination. Simultaneously, DOX was released and activated with high controllability by light to significantly enhance the therapeutic efficacy and minimize the side effect [26]. Tosi et al. have synthesized ROS-responsive conjugate, namely, mPEG-TK-Cy5, and demonstrated that, differently to non-ROS-responsive control conjugate (mPEG-Cy5), mPEG-TK-Cy5 showed a selective release of Cy5 in response to ROS in both, ROS-simulated conditions, and *in vitro* on glioblastoma cells [27].

Herein, in this study, we integrated the mitochondria-targeting moieties and ROS-triggered groups into the nano-PDT system. Detailedly, we have synthesized amphiphilic triphenylphosphonium- (TPP-) PEG linked chlorin e6 (Ce6) via ROS-responsive thioketal (TK) bonds (TPPPEG-TK-Ce6), which could self-assemble into spherical nanoparticles. Furthermore, the release behaviors, cell cytotoxicity, and intracellular distribution of Ce6 were comprehensively investigated.

2. Materials and Methods

2.1. Materials. 3-Mercaptopropionic acid and ethanediamine were purchased from Sinopharm Chemical Reagent Co. Ltd. (China). Acetone and CH_2Cl_2 were distilled before use. Ce6, 5-bromovaleric acid (Br-C_4H_8-COOH), triphenylphosphine, polyethylene glycol 2000 (PEG_{2000}), polyethylene glycol monomethyl ether 2000 ($mPEG_{2000}$), methanesulfonyl chloride, 4-dimethylaminopyridine (DMAP), N,N'-dicyclohexylcarbodiimide (DCC), 3-[4, 5-dimethylthiazol-2-yl]-2, 5-diphenyltetrazolium bromide (MTT), dichlorofluorescein diacetate (DCFH-DA), and dimethylsulfoxide (DMSO) were obtained from Sigma-Aldrich (St. Louis, USA). RPMI1640 medium, fetal bovine serum (FBS), antibiotic penicillin/streptomycin, and trypsinase were obtained from Gibco BRL (Grand Island, USA). Hoechst 33258, MitoTracker® Red, MitoTracker® Green, and Mitotracker® Red CMXRos were purchased from Invitrogen (Eugene, OR, USA). Other chemicals if not specified were all commercially available and used as received. C6 cells were purchased from Chinese Typical Culture Center (CTCC) (Wuhan University, China) and cultured in RPMI1640 supplemented with 10% FBS and 1% antibiotics (100 U mL^{-1} penicillin and 100 μg mL^{-1} streptomycin) at 37°C in a humidified air atmosphere containing 5% CO_2. Milli-Q water, with a resistivity of 18.2 MΩ cm^{-1}, was obtained by a Milli-Q Plus gradient system (Millipore Corporation, Bedford, USA) and used for all the experiments.

2.2. Synthesis and Characterization. The synthesis procedures of NH_2-PEG-NH_2 (1), 4-carboxbutyltriphenylphosphonium bromide (TPP-C_4-COOH, 2), TPP-PEG-NH_2 (3), and HOOC-TK-COOH (4) are according to the reported work [12].

TPP-PEG-TK-COOH (5): HOOC-TK-COOH (0.126 g) with 0.060 g of DMAP and 0.110 g of DCC was dissolved in anhydrous dichloromethane. Then, 1.229 g of TPP-PEG-NH_2 was added into the mixture and stirred for 12 h at room temperature. Finally, the products were precipitated by icy ether and dried in vacuum, yield 64.47%.

TPP-PEG-TK-NH_2 (6): 0.737 g of TPP-PEG-TK-COOH with 0.036 g of DMAP and 0.063 g of DCC was dissolved in 25 mL of anhydrous dichloromethane and stirred for 1 h. Then, excessive ethylenediamine was added into the mixture and further stirred for another 12 h at room temperature. The mixture was precipitated by icy ether and dried in vacuum, yield 44.99%.

The amphiphilic copolymer containing TPP and TK groups (TPP-PEG-TK-COOH-Ce6, 7): 0.060 g of Ce6 with 0.012 g of DMAP and 0.021 g of DCC was dissolved in 25 mL of anhydrous tetrahydrofuran in dark. After that, 0.277 g of TPP-PEG-TK-NH_2 in 10 mL of anhydrous tetrahydrofuran was slowly added into the mixture and reacted for 12 h at room temperature in dark. Then, the mixture was precipitated by icy ether, and the obtained product was further dialyzed against distilled water for 72 h in a dialysis tube (MWCO 3500 cutoff) and dried in vacuum, yield 54.8%. The controls of the amphiphilic copolymer without TPP group or TK group were synthesized as before by replacing TPP-PEG-NH_2 and HOOC-TK-COOH with mPEG-NH_2 and oxalic acid, respectively.

Characterization: ^{1}H nuclear magnetic resonance (^{1}H NMR) spectra were recorded on a Varian Unity 300 MHz spectrometer (Varian, USA) and tetramethyl silane as an internal standard.

2.3. Preparation of Micelles. Micelles were prepared by dialysis. Briefly, 20 mg of amphiphilic copolymer was dissolved in 4 mL of DMSO. Then, the solution was transferred to a dialysis tube (MWCO 3500 cutoff) and dialyzed against distilled water for 72 h. The dialysis water was exchanged every 4 h on the first day, and then every 12 h in the following 48 h. After that, the mixture was stored at 4°C before use, and the entire procedure was carried out in the dark. The obtained micelles with TPP (mitochondrial-targeting) and TK groups (ROS-triggered) were designated as TRM, micelles without TPP group were designated as RM, and micelles without TK groups were designated as TM.

2.4. Characterization of the Micelles. The average hydrodynamic particle sizes, polydispersity index (PDI), and zeta potential of the micelles in phosphate-buffered saline (PBS, 10 mM, pH 7.4) were monitored by a ZETA-SIZER Nano Series ZEN3600 (Malvern Instruments Ltd, UK). The

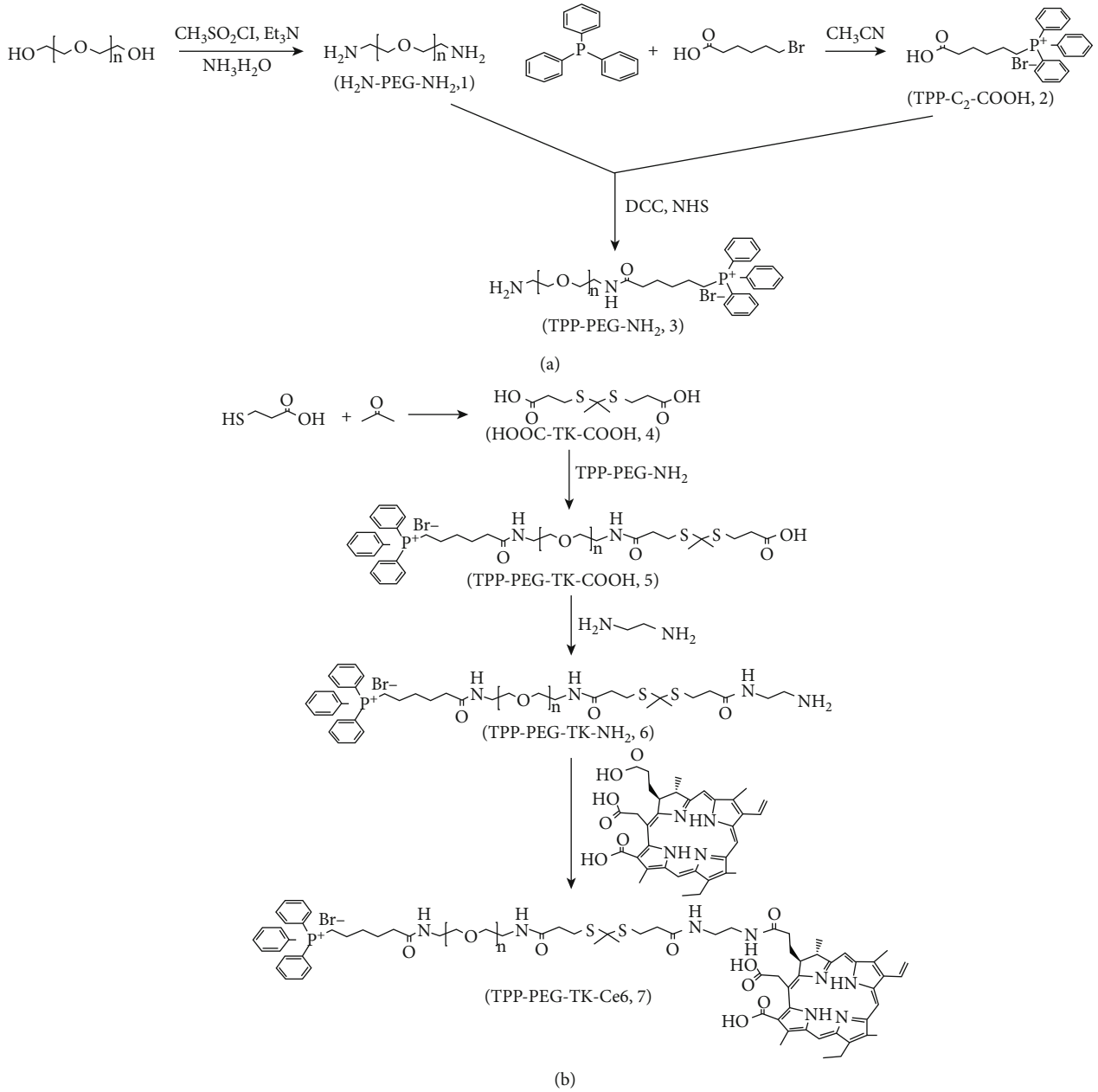

Figure 1: The synthesis pathway of TPP-PEG-NH_2 (a), HOOC-TK-COOH (b), and the amphiphilic copolymer of TPP-PEG-TK-Ce6 (c)

morphology of the polymeric micelles was carried out on a JEM 2010 FEF transmission electron microscope (TEM, JEOL, Japan).

2.5. Cytotoxicity Assay. The cell viability of TRM, TM, and RM was evaluated against C6 cells by MTT assay. Typically, the cells were seeded into 96-well plates at a density of 5×10^3 cells per well and incubated in 100 μL RPMI1640 containing 10% FBS at 37°C in 5% CO_2 atmosphere for 24 h. Another 100 μL micelles dispersed in culture medium with various concentrations of Ce6 were separately added into each well. After the micelles were incubated with cells for 24 h, the medium was removed. The cells were washed thrice with PBS to remove noninternalized nanoparticles, and 200 μL fresh culture medium was added to each well. Then, the cells were irradiated with LED light (630 nm, 30 mW cm^{-2}, 5 min) or not, and the cells were further cultured for another 24 h. Subsequently, 100 μL culture medium and 20 μL MTT solution (5 mg mL^{-1} in PBS) were added to each well and further incubated for 4 h at 37°C. After that, the medium was replaced by 150 μL DMSO to dissolve the formazan blue crystal. The absorbance of the solution was measured at 570 nm using a microplate reader (Versa max, USA).

Cell viability was expressed as follows:

$$\text{Cell viability } (\%) = \frac{\text{OD}_{\text{sample}}}{\text{OD}_{\text{control}}} \times 100\%, \quad (1)$$

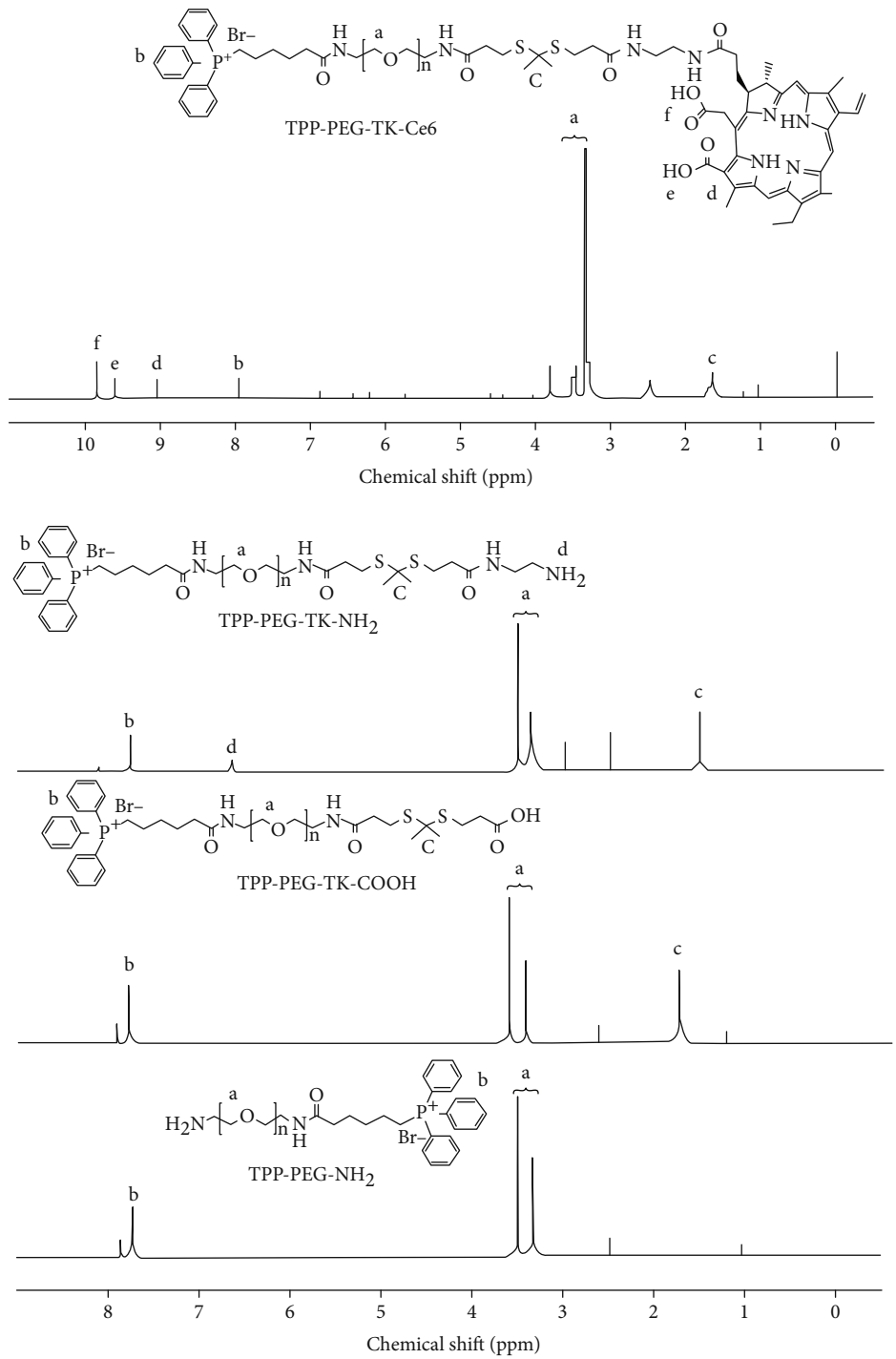

Figure 2: ^{1}H NMR spectra of TPP-PEG-NH_2, TPP-PEG-TK-COOH, TPP-PEG-TK-NH_2, and TPP-PEG-TK-Ce6 in DMSO-D6 at 25°C.

where OD_{sample} and $OD_{control}$ are the absorbance values of the treated cells and the untreated control cells, respectively, which were obtained after subtracting the absorbance of DMSO.

2.6. Confocal Laser Scanning Microscope (CLSM). C6 cells were seeded in confocal dishes at a density of 5.0×10^4 cells per well and cultured for 24 h. Then, the cells were separately treated with TRM, TM, and RM, according to 2 μg mL^{-1} Ce6. After 4 h incubation, the culture medium was removed, and the cells were washed thrice with PBS7.4 to remove noninternalized nanoparticles. Then, the cells were irradiated with LED light (630 nm, 30 mW cm^{-2}, 5 min). Later, the cells were stained with 200 μL Hoechst 33258 (5 μg mL^{-1} in PBS) for 10 min, further stained by 1 mL Mitotracker® Green (100 nM) for 15 min, and were rinsed with PBS thrice for CLSM. Simultaneously, the quantitative experiments were conducted. After treatment with the same samples, the cells

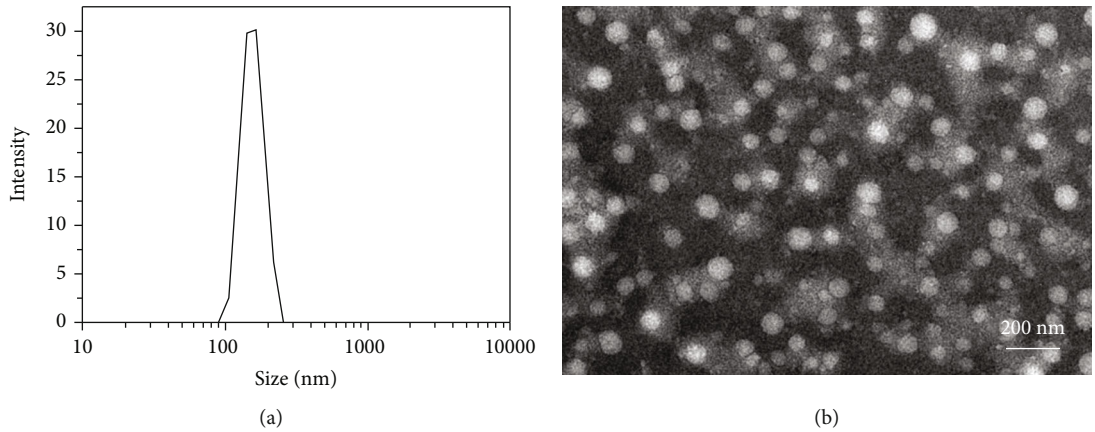

Figure 3: Size distributions of TRM measured by DLS (a) and the TEM image of TRM (b). Scale bar was 200 nm.

were washed with PBS thrice, trypsinized for 1 min, and resuspended in 600 μL distilled water. 500 μL cell suspension was centrifuged to collect cells for the assay of quantitative cellular uptake. The collected cells were broken by Triton X-100, and the supernatant was collected for fluorescence measurement. The protein concentration was determined by the remaining 100 μL cell suspension, which was examined by a BCA assay kit. The quantitative intracellular Ce6 contents were determined by the fluorescence values of Ce6 normalized against the corresponding protein concentration.

After the cells incubated by micelles (2 μg mL^{-1} Ce6) for 4 h, 1 mL Mitotracker® Green CMXRos (100 nM) was added into the dish and incubated in DMEM for 20 min. After that, the cells were washed by DMEM, further incubated in DMEM containing 10% FBS for 10 min and irradiated by LED light. Finally, the cells were further stained by Mitotracker® Red and Hoechst 33258 for 15 min, respectively, washed and observed by CLSM. For quantitative analysis, the procedure was similar as that for the CLSM imaging of intracellular ROS. After illumination, 0.5 mL of trypsin-EDTA solution (0.25%) was added to detach the cells, blown down with DMEM containing 10% FBS, and then centrifuged (1000 rpm, 5 min). The collected cells were washed by PBS thrice and analyzed by flow cytometer (CyAN-ADP, Beckman). The excitation wavelength was 488 nm, and the emission filter was at 525 nm.

3. Results and Discussion

3.1. Synthesis and Characterization of TPP-PEG-TK-Ce6. To synthesize amphiphilic TPP-PEG-TK-Ce6, TPP-PEG-NH_2 was firstly reacted with HOOC-TK-COOH, then, chemically transferred carboxyl-terminated TPP-PEG-TK-COOH into amino-terminal TPP-PEG-NH_2 via reacting with ethylenediamine (TPP-PEG-TK-NH_2). Subsequently, TPP-PEG-TK-NH_2 was further conjugated with Ce6 (Figure 1).

The ^{1}H NMR spectrum of TPP-PEG-NH_2, TPP-PEG-TK-COOH, TPP-PEG-TK-NH_2, and TPP-PEG-TK-Ce6 is shown in Figure 2. The proton peak a that appeared at δ 3.5-3.7 ppm was observed, which indicated the distinct PEG peaks. The proton peaks of b at δ 7.5-7.9 ppm were assigned to the presence of TPP moieties. The peaks of c observed at δ 1.4-1.8 ppm were assigned to the methyl groups of TK. The appearance of peak d at δ 6.7 ppm of TPP-PEG-TK-NH_2 indicated the distinct -NH_2 groups when TPP-PEG-TK-COOH chemically modified into amino-terminated TPP-PEG-TK-NH_2. Finally, after TPP-PEG-TK-NH_2 conjugated with Ce6, the distinct peaks f and d at δ 9.6-10 ppm were assigned to the carboxyl groups of TPP-PEG-TK-Ce6. All these representative peaks in the results of ^{1}H NMR spectrum of TPP-PEG-NH_2, TPP-PEG-TK-COOH, TPP-PEG-TK-NH_2, and TPP-PEG-TK-Ce6 demonstrated the successful synthesis of TPP-PEG-TK-Ce6. The Ce6 content of the amphiphilic copolymer was calculated by the peak of TK bond and the characteristic peak of Ce6, which was 1.06 : 1 and calculated the content of Ce6 was 17.6%.

3.2. Preparation and Characterization of the Micelles. Amphiphilic copolymers could self-assemble into micelles with core-shell structure. The micelles of TRM were self-assembled from the amphiphilic copolymers of TPP-PEG-TK-Ce6 by dialysis via solvent exchange. As shown in Figure 3(a), dynamic light scattering (DLS) results revealed that TPP-PEG-TK-Ce6 aggregated into monodisperse nanoparticles with an average particle size of 160 nm (PDI = 0.288), and the zeta potential was +20.1 mV. The morphology of TRM was further examined by TEM, which confirmed that the amphiphilic copolymers of TPP-PEG-TK-Ce6 could self-assembled into approximate spherical nanoparticles in water, and their average diameter was close to 150 nm (Figure 3(b)), which was consistent with the results of DLS detection. Moreover, the average particle size of the controls of TM and RM was 158 nm and 166.4 nm with zeta potential of +21.2 mV and +12.4 mV, respectively.

3.3. In Vitro Release Behaviors. The capability of light-activated release property of TRM is a vital role that influences the antitumor therapeutic effects [29–31]. The ROS-responsive release behaviors of Ce6 from the micelles were evaluated in simulated physiological environment (PBS7.4) by irradiated with a LED light for 5 min. As shown in Figure 4(a), the release of Ce6 from TM after 60 h was less than 9% both with or without illumination. However, the

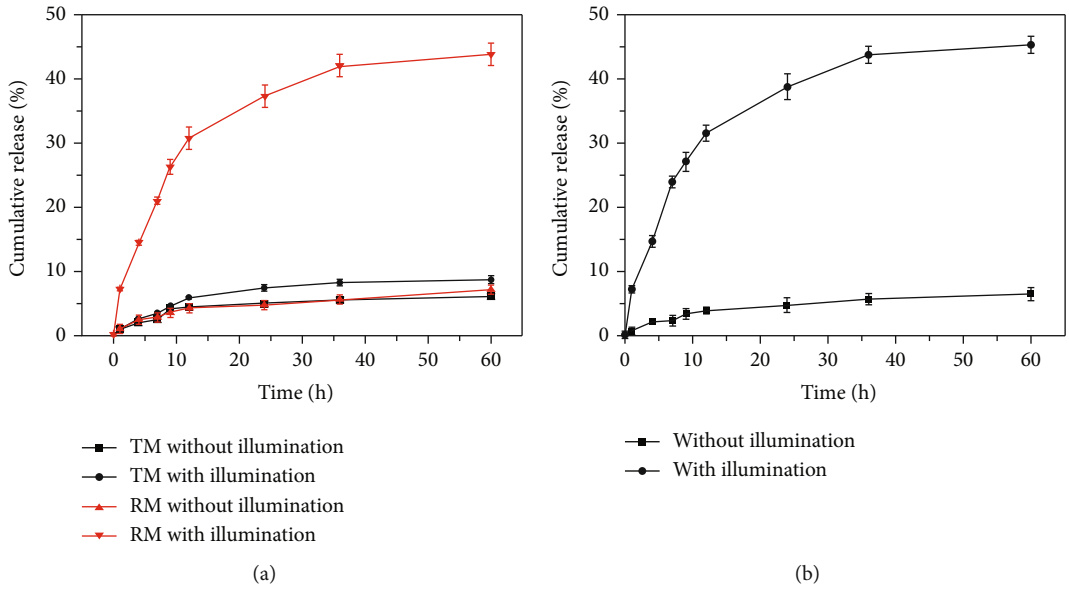

Figure 4: The release profiles of Ce6 from the controls of TM and RM (a) and TRM (b).

release of Ce6 from RM after 60 h without or with light irradiation was 7.3% and 43.8%, respectively, which demonstrated that the release behaviors of Ce6 from RM micelles showed a light-activated release way. Moreover, the release of Ce6 from TRM after 60 h without illumination was only 6.4%, however, under light irradiation, the amount of released Ce6 reached 45.3%, which also exhibited the light-activated release behaviors. The controlled release behaviors on light-activation could be attributed to the ROS cleavage of TK linkages in RM and TRM. These results indicated that the *in vitro* release behaviors of Ce6 from RM and TRM exhibited ROS responsiveness which may lead to site-specific controlled release by light-activation in tumor microenvironment.

3.4. Cytotoxicity. The effect of light irradiation on the cytotoxicity of TM, RM, and TRM was investigated on C6 cells (cancerous cells) using MTT assay. As shown in Figure 5, all of TM, RM, and TRM were noncytotoxic to C6 cells when without light irradiation. In addition, even under illumination of 630 nm (30 mW cm^{-2}) laser for 5 min, TM also showed a negligible cytotoxicity to C6 cells. Whereas, after irradiation, both of RM and TRM were more toxic to C6 cells than that without illumination, which showed an obvious light-activated cytotoxicity to C6 cells. Moreover, when the Ce6 concentration was 2 $\mu g\,mL^{-1}$, the cell viability of RM and TRM decreased to 36.3% and 22.5%, respectively (Figure 5), which exhibited a dose-dependent cytotoxicity of RM and TRM to C6 cells. The highest cytotoxicity of TRM (IC_{50} = 1.08 $\mu g\,mL^{-1}$) than that of TM and RM indicated that the PDT efficacy could further elevated by mitochondrial-targetability of TPP moieties and ROS-triggered release of Ce6 in cancerous cells.

3.5. CLSM. To further investigate the subcellular distribution, the mitochondria of C6 cells after treatment with TM,

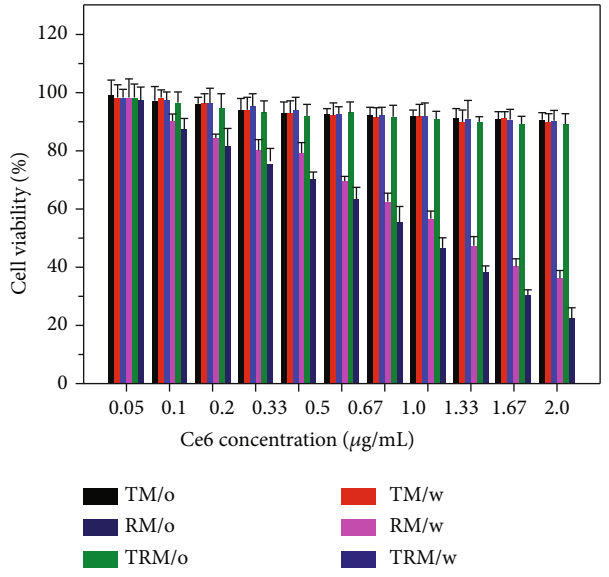

Figure 5: Dose-dependent cell viability of C6 cells with incubation of TM, RM and TRM under a 630 nm laser treatment for 5 min at 30 mW/cm^2 (n = 3).

RM, and TRM for 4 h were stained by Mito-Tracker Green and observed by CLSM. As shown in Figure 6, intracellular Ce6 and mitochondria were indicated as red fluorescence and green dots, respectively. In the case of treating C6 cells with RM, no obvious mitochondrial accumulation was observed because of the rare red dots, whereas, significant red fluorescence was located in the nucleus of C6 cells (Figure 6). However, distinct yellow dots representing the colocalization of green and red dots could be found in the merged images of TM and TRM treated cells, demonstrating the successful colocalization between Ce6 and mitochondria. Moreover, the highest red fluorescence was found in the

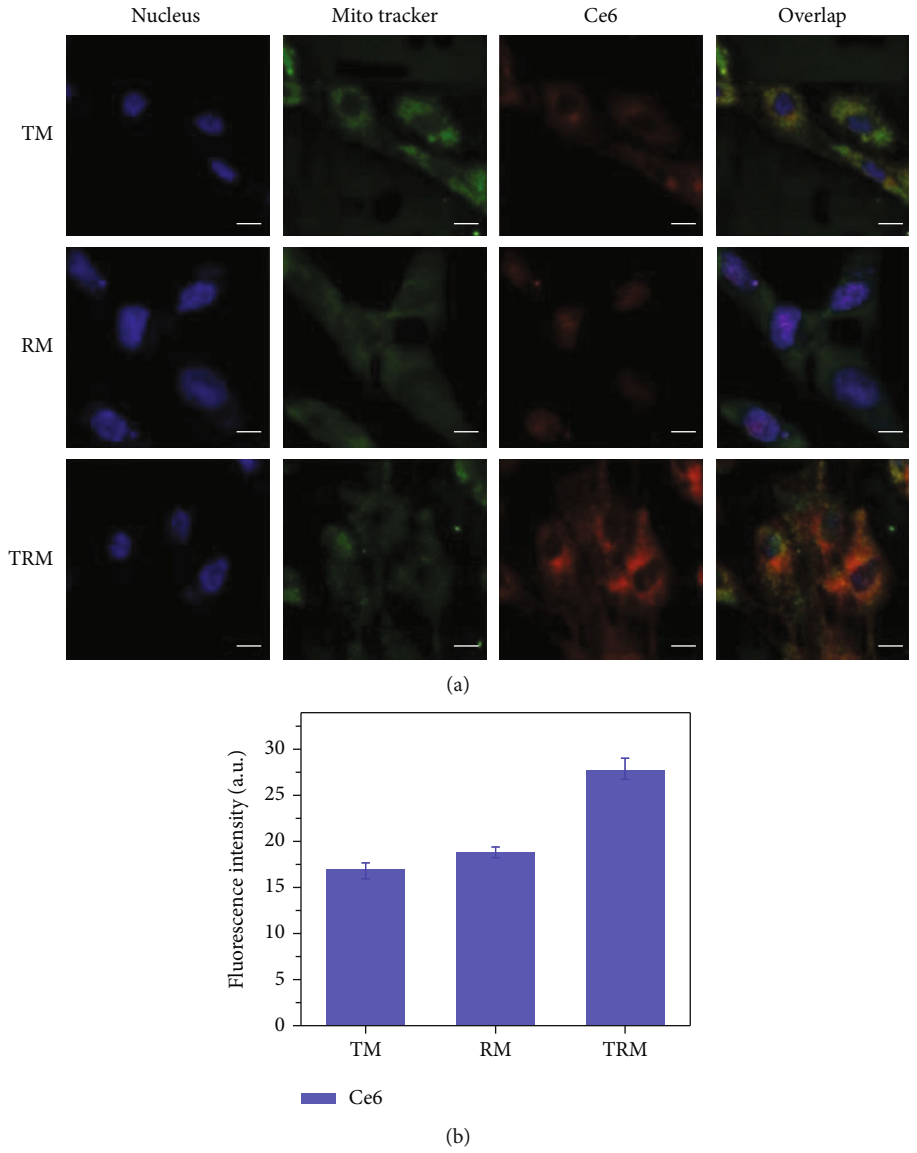

Figure 6: (a) CLSM images of C6 cells and intracellular ROS generation after treating with TM, RM, and TRM for 4 h with laser irradiation. Scale bar was 20 μm. (b) The fluorescence intensity of Ce6 delivered into tumor cells by different nanoparticles.

mitochondria of C6 cells treated with TRM. Furthermore, the fluorescence intensity of Ce6 that was delivered into C6 cells by different nanoparticles was calculated by Image J. These quantified results were consistent with the fluorescence images, where TRM delivered more Ce6 into C6 cells in comparison with TM and RM nanoparticles. These results indicated that more efficient delivery of Ce6 into mitochondria by TRM stemmed from a combination of the better cellular accumulation caused by the mitochondria-targeting ability of TPP groups via the electrostatic interaction between the positively charged TRM and mitochondrial membrane and ROS-triggered release of Ce6 in the mitochondria.

4. Conclusion

A new kind of amphiphilic copolymer with mitochondria-targeting and ROS-responsive characteristics was synthesized and self-assembled into micelles for *in vitro* PDT. The micelles showed ROS-responsive release of Ce6 under light irradiation and could efficiently accumulated in the mitochondria of C6 cells and release Ce6 via ROS triggering, which exhibited good cytotoxicity to C6 cells. This research provided a new method for developing mitochondria-targeting delivery systems for PDT.

Data Availability

The data used to support the findings of this study are available from the corresponding author upon request.

Conflicts of Interest

The authors declare that there is no conflict of interest regarding the publication of this paper.

Authors' Contributions

Yangjian Wang and Junshui Zheng contributed equally to this work.

Acknowledgments

Financial support for this work is provided by Medical Health Science and Technology Project of Zhejiang Provincial Health Commission (2019KY569) and Ningbo "Science and technology innovation 2025" third batch of major special science and technology projects (2019B10104).

References

[1] D. M. Ozog, A. M. Rkein, S. G. Fabi et al., "Photodynamic therapy: a clinical consensus guide," *Dermatologic Surgery*, vol. 42, no. 7, pp. 804–827, 2016.

[2] M. J. Manyak, A. Russo, P. D. Smith, and E. Glatstein, "Photodynamic therapy," *Journal of Clinical Oncology*, vol. 6, no. 2, pp. 380–391, 1988.

[3] B. G. Yi, O. K. Park, M. S. Jeong et al., "*In vitro* photodynamic effects of scavenger receptor targeted-photoactivatable nanoagents on activated macrophages," *International Journal of Biological Macromolecules*, vol. 97, pp. 181–189, 2017.

[4] S. Kwiatkowski, B. Knap, D. Przystupski et al., "Photodynamic therapy - mechanisms, photosensitizers and combinations," *Biomedicine & Pharmacotherapy*, vol. 106, pp. 1098–1107, 2018.

[5] C. Donohoe, M. O. Senge, L. G. Arnaut, and L. C. Gomes-da-Silva, "Cell death in photodynamic therapy: from oxidative stress to anti-tumor immunity," *Biochimica Et Biophysica Acta. Reviews on Cancer*, vol. 1872, no. 2, article 188308, 2019.

[6] L. Nguyen, M. Li, S. Woo, and Y. You, "Development of prodrugs for PDT-based combination therapy using a singlet-oxygen-sensitive linker and quantitative systems pharmacology," *Journal of Clinical Medicine*, vol. 8, no. 12, p. 2198, 2019.

[7] D. A. Bellnier, W. R. Greco, G. M. Loewen, H. Nava, A. R. Oseroff, and T. J. Dougherty, "Clinical pharmacokinetics of the PDT photosensitizers porfimer sodium (Photofrin), 2-[1-hexyloxyethyl]-2-devinyl pyropheophorbide-a (Photochlor) and 5-ALA-induced protoporphyrin IX," *Lasers in Surgery and Medicine*, vol. 38, no. 5, pp. 439–444, 2006.

[8] X. Li, S. Lee, and J. Yoon, "Supramolecular photosensitizers rejuvenate photodynamic therapy," *Chemical Society Reviews*, vol. 47, no. 4, pp. 1174–1188, 2018.

[9] U. Chilakamarthi and L. Giribabu, "Photodynamic therapy: past, present and future," *The Chemical Record*, vol. 17, no. 8, pp. 775–802, 2017.

[10] L. Zhang, Y. Qi, H. Min et al., "Cooperatively responsive peptide nanotherapeutic that regulates angiopoietin receptor Tie2 activity in tumor microenvironment to prevent breast tumor relapse after chemotherapy," *ACS Nano*, vol. 13, no. 5, pp. 5091–5102, 2019.

[11] Z. Zhou, J. Song, L. Nie, and X. Chen, "Reactive oxygen species generating systems meeting challenges of photodynamic cancer therapy," *Chemical Society Reviews*, vol. 45, no. 23, pp. 6597–6626, 2016.

[12] N. Peng, H. Yu, W. Yu et al., "Sequential-targeting nanocarriers with pH-controlled charge reversal for enhanced mitochondria-located photodynamic-immunotherapy of cancer," *Acta Biomaterialia*, vol. 105, pp. 223–238, 2020.

[13] R. E. Koch, C. C. Josefson, and G. E. Hill, "Mitochondrial function, ornamentation, and immunocompetence," *Biological Reviews of the Cambridge Philosophical Society*, vol. 92, no. 3, pp. 1459–1474, 2017.

[14] Z. W. Zhang, X. C. Xu, T. Liu, and S. Yuan, "Mitochondrion-permeable antioxidants to treat ROS-burst-mediated acute diseases," *Oxidative Medicine and Cellular Longevity*, vol. 2016, Article ID 6859523, 10 pages, 2016.

[15] J. Nunnari and A. Suomalainen, "Mitochondria: in sickness and in health," *Cell*, vol. 148, no. 6, pp. 1145–1159, 2012.

[16] M. T. Lin and M. F. Beal, "Mitochondrial dysfunction and oxidative stress in neurodegenerative diseases," *Nature*, vol. 443, no. 7113, pp. 787–795, 2006.

[17] V. Sorrentino, K. J. Menzies, and J. Auwerx, "Repairing mitochondrial dysfunction in disease," *Annual Review of Pharmacology and Toxicology*, vol. 58, no. 1, pp. 353–389, 2018.

[18] Z. Liu, H. Zou, Z. Zhao et al., "Tuning organelle specificity and photodynamic therapy efficiency by molecular function design," *ACS Nano*, vol. 13, no. 10, pp. 11283–11293, 2019.

[19] Y. Shen, A. J. Shuhendler, D. Ye, J. J. Xu, and H. Y. Chen, "Two-photon excitation nanoparticles for photodynamic therapy," *Chemical Society Reviews*, vol. 45, no. 24, pp. 6725–6741, 2016.

[20] F. J. Bock and S. W. G. Tait, "Mitochondria as multifaceted regulators of cell death," *Nature Reviews. Molecular Cell Biology*, vol. 21, no. 2, pp. 85–100, 2020.

[21] J. Chen, T. Fan, Z. Xie et al., "Advances in nanomaterials for photodynamic therapy applications: status and challenges," *Biomaterials*, vol. 237, p. 119827, 2020.

[22] B. Ozsvari, F. Sotgia, and M. P. Lisanti, "Exploiting mitochondrial targeting signal(s), TPP and bis-TPP, for eradicating cancer stem cells (CSCs)," *Aging (Albany NY)*, vol. 10, no. 2, pp. 229–240, 2018.

[23] R. Mo, Q. Sun, J. Xue et al., "Multistage pH-responsive liposomes for mitochondrial-targeted anticancer drug delivery," *Advanced Materials*, vol. 24, no. 27, pp. 3659–3665, 2012.

[24] Y. Zhang, B. Wang, R. Zhao, Q. Zhang, and X. Kong, "Multifunctional nanoparticles as photosensitizer delivery carriers for enhanced photodynamic cancer therapy," *Materials Science & Engineering. C, Materials for Biological Applications*, vol. 115, p. 111099, 2020.

[25] M. Lan, S. Zhao, W. Liu, C. S. Lee, W. Zhang, and P. Wang, "Photosensitizers for photodynamic therapy," *Advanced Healthcare Materials*, vol. 8, no. 13, article e1900132, 2019.

[26] P. Pei, C. Sun, W. Tao, J. Li, X. Yang, and J. Wang, "ROS-sensitive thioketal-linked polyphosphoester-doxorubicin conjugate for precise phototriggered locoregional chemotherapy," *Biomaterials*, vol. 188, pp. 74–82, 2019.

[27] N. Oddone, F. Pederzoli, J. T. Duskey et al., "ROS-responsive "smart" polymeric conjugate: synthesis, characterization and proof-of-concept study," *International Journal of Pharmaceutics*, vol. 570, p. 118655, 2019.

[28] S. S. Wan, J. Y. Zeng, H. Cheng, and X. Z. Zhang, "ROS-induced NO generation for gas therapy and sensitizing photodynamic therapy of tumor," *Biomaterials*, vol. 185, pp. 51–62, 2018.

[29] E. Menares, F. Gálvez-Cancino, P. Cáceres-Morgado et al., "Tissue-resident memory $CD8^+$ T cells amplify anti-tumor

immunity by triggering antigen spreading through dendritic cells," *Nature Communications*, vol. 10, no. 1, p. 4401, 2019.

[30] C. Li, B. Zhu, Y. M. Son et al., "The transcription factor Bhlhe40 programs mitochondrial regulation of resident $CD8^+$ T cell fitness and functionality," *Immunity*, vol. 51, no. 3, pp. 491–507.e7, 2019, e7.

[31] M. Enamorado, S. Iborra, E. Priego et al., "Enhanced anti-tumour immunity requires the interplay between resident and circulating memory $CD8^+$ T cells," *Nature Communications*, vol. 8, no. 1, article 16073, 2017.